A Monte Carlo Model of Piezoelectric Scattering in GaN

S. Vitanov, M. Nedjalkov, and V. Palankovski

Advanced Materials and Device Analysis Group, Inst. for Microelectronics, TU Wien, Gusshausstrasse 27-29, A-1040 Vienna, Austria

Abstract. A non-parabolic piezoelectric model of electron-phonon interaction in Gallium Nitride is discussed. The Monte Carlo aspects of the model, needed for the simulation tools which provide the characteristics of GaN-based devices are analyzed in details. The piezo-scattering rate is derived by using quantum-mechanical considerations. The angular dependence is avoided by a proper spherical averaging and the non-parabolicity of the bands is accounted for. For the selection of the after-scattering state we deploy the rejection technique. The model is implemented in a simulation software. We employ a calibrated experimentally verified set of input material parameters to obtain valuable data for the transport characteristics of GaN. The simulation results are in good agreement with experimental data available for different physical conditions.

1 Introduction

Gallium Nitride (GaN) based devices demonstrate impressive power capabilities in radio-frequency range which recently became of interest for applications in state-of-the-art mobile communication technology, e.g. base stations amplifiers. The physical model of GaN, needed for the Monte Carlo (MC) simulation tools to describe the electronic and optical behavior of this material, is subject of an active research and development [1], [2], [3]. The model provides information about the band structure (analytical or full-band), the scattering mechanisms (caused by impurities, acoustic and optical phonons) and other microscopic characteristics which govern the carrier transport in the semiconductor.

There are two types of GaN crystal lattice structures: wurtzite or zink blende. Due to the the lack of inversion symmetry, elastic strain gives rise to macroscopic electric fields. These fields cause additional coupling between the acoustic waves and the free carriers, known as piezoelectric scattering. Nitrides are characterized by the largest piezoelectric constants among the III-V semiconductors so that this scattering must be taken into account in the MC simulations. The papers related to this subject stress on the simulation results and merely formulate the out-scattering rate of the utilized piezo-model. The next section of this work focuses on the MC aspects and peculiarities of a non-parabolic piezo-scattering model. The simulation results obtained by the proposed MC approach are discussed in the last section.

T. Boyanov et al. (Eds.): NMA 2006, LNCS 4310, pp. 197–204, 2007.

2 The Model

According the Golden rule the probability for scattering from electron state $\mathbf{k}$ to state $\mathbf{k}'$ by phonons with wave vector $\mathbf{q}$ in branch j is determined with the help of the matrix element $|\langle \mathbf{k}', \hat{n}'_{\mathbf{q},j}|H_{e-p}|\hat{n}_{\mathbf{q},j}, \mathbf{k}\rangle|^2\delta(E - E')$. Standard notations are used, where H_{e-p} is the interaction Hamiltonian $|\hat{n}, \mathbf{k}\rangle$ denotes the electron-phonon state, $\hat{n}$ and $\hat{n}'$, and E and E', refer to the initial and final phonon number and energies respectively. Phonons are described by waves $\mathbf{s} = \mathbf{e}\exp(i\mathbf{q}.\mathbf{r} - \omega_q t)$ where $\mathbf{r}$ is the position, ω_q the energy and $\mathbf{e}$ the unit vector of the polarization[1]. The basic piezo-interaction energy is proportional to the integral of the electric displacement $\mathbf{D}(\mathbf{r})$ associated with the electron, multiplied by the lattice polarization $\mathbf{P}(\mathbf{r})$. The screening is accounted via the Thomas-Fermi model, which introduces in $\mathbf{D}$ the reciprocal Debye screening length q_0. The polarization is proportional to the strain $\mathbf{S}$ caused by the propagating acoustic waves: $\mathbf{P}_i = \sum_{ik} e_{ik}\mathbf{S}_k/\epsilon_r$ where, in reduced notations i, k run from 1 to 6, e_{ik} denote the piezo coefficients, and ϵ_r is the dielectric constant. For zinc blende crystals $e_{14} = e_{25} = e_{36}$ and all other components are zero. For wurtzite only $e_{15} = e_{24}$, $e_{31} = e_{32}$ and e_{33} are non-zero. The matrix element of H_{e-p} gives rise to conservation rules for the phonon numbers: $n' = n \pm 1$ and the electron wave vector $\mathbf{k}' = \mathbf{k} \pm \mathbf{q}$. The Bloch assumption [4] allows to replace the phonon degrees of freedom with their mean equilibrium number $n_{\mathbf{q}}$ given by the Bose-Einstein distribution. The factor $H'(e_{kl}, \mathbf{e}, \alpha, \beta, \gamma, q_0, q)$ summarizes the complicated dependence of the matrix element on the polarization $\mathbf{e}$ and direction cosines α, β, γ of the direction of propagation of $\mathbf{q}$ with respect to the crystal axes. A simplification is certainly desirable and is achieved by a spherical averaging. The averaged scattering rate W can be written explicitly as:

$$W = W_a + W_e = \sum_{\pm} \frac{2\pi}{\hbar}|F(q)|^2(n_q + \frac{1}{2} \mp \frac{1}{2})\delta\left(\epsilon(\mathbf{k} \pm \mathbf{q}) \mp \epsilon(\mathbf{k}) \mp \hbar\omega_q\right) \qquad (1)$$

where W_a corresponds to absorption ($\mathbf{k}' = \mathbf{k}+\mathbf{q}$) and W_e to emission ($\mathbf{k}' = \mathbf{k}-\mathbf{q}$) of a phonon with wave vector $\mathbf{q}$. The averaged isotropic coupling constant depends on q as $|F(q)|^2 = Cf(q)$, $f(q) = \frac{q^3}{(q^2+q_0^2)^2}$. The constant C will be introduced later.

We consider a three valley (Γ, U, and L) spherical non-parabolic energy dispersion model with m the effective electron mass for the corresponding valley:

$$\frac{\hbar^2k^2}{2m} = \epsilon(k)(1 + \alpha\epsilon(k)) = \gamma(k); \qquad k = \frac{1}{\hbar}\sqrt{2m\gamma}; \qquad \mathbf{v}(\mathbf{k}) = \frac{\hbar\mathbf{k}}{m(1 + 2\alpha\epsilon(k))}$$

2.1 Absorption

The absorption out-scattering rate $\lambda_a = \int W_a d\mathbf{k}'$ is calculated by using spherical coordinates (q, θ, ϕ), where the z axis is chosen along $\mathbf{k}$ so that θ becomes the angle between $\mathbf{k}$ and $\mathbf{q}$:

[1] In an isotropic media there are one longitudinal, L, ($\mathbf{e}||\mathbf{q}$) and two transverse, T, $\mathbf{e} \perp \mathbf{q}$ branches. In crystals L and T exist for special directions only.

$$\lambda_a = \frac{V2\pi C}{(2\pi)^3\hbar}\int_0^{2\pi} d\phi \int_{-1}^{1} d\cos\theta \int_0^{\infty} dq q^2 f(q) n_q \delta(\epsilon(k,q,\theta) + \epsilon(k) - \hbar\omega_q)$$

where $\frac{V}{(2\pi)^3}$ is the density of states in the $\mathbf{q}$ space. The acoustic phonon energy $\hbar\omega_{\mathbf{q}} = \hbar v_s q$ introduces the sound velocity v_s which is anisotropic. The following consideration can be applied if a particular direction of $\mathbf{q}$ is considered, or if a spherical average is taken for v_s. The argument of the delta function becomes zero if

$$\cos\theta = \frac{2v_s}{v(k)} - \frac{q}{2k}(1 - 4\alpha\epsilon_s); \qquad \epsilon_s = \frac{mv_s^2}{2}$$

which, furthermore, gives rise to the following condition for $q_1 \le q \le q_2$:

(i) if $\frac{v_s}{v} < 1$ then $-1 \le \cos\theta \le \frac{v_s}{v}$ and $q_1 = 0$, $q_2 = \frac{2k(v_s/v+1)}{1-4\alpha\epsilon_s}$;
(ii) else $-1 \le cos\theta \le 1$ and $q_1 = \frac{2k(v_s/v-1)}{1-4\alpha\epsilon_s}$, $q_2 = \frac{2k(v_s/v+1)}{1-4\alpha\epsilon_s}$.

By using the equipartition approximation: $n_q = kT/\hbar\omega_q = kT/\hbar v_s q$ and introducing the dimensionless variable $x = q/q_0$ ($x_i = q_i/q_0$), the scattering rate is obtained:

$$\lambda_a = \underbrace{\frac{\mathrm{e}^2 K_{av}^2\sqrt{m}kT}{8\pi\epsilon_0\epsilon_r\hbar^2\sqrt{2\gamma(k)}}(1 + 2\alpha\epsilon(k))}_{C_1(k)} I_1(x_1,x_2) + \underbrace{\frac{\mathrm{e}^2 v_s K_{av}^2\sqrt{m}2\alpha kTq_0}{8\pi\epsilon_0\epsilon_r\hbar\sqrt{2\gamma(k)}}}_{C_2(k)} I_2(x_1,x_2)$$

where e is the electric charge and the integrals I_1 and I_2 are evaluated as follows:

$$I_1 = \int_{x_1}^{x_2} dx \frac{x^3}{(x^2+1)^2} = \int_{x_1}^{x_2} J_1(x)dx; \quad I_2 = \int_{x_1}^{x_2} dx \frac{x^4}{(x^2+1)^2} = \int_{x_1}^{x_2} J_2(x)dx$$

The coefficients $C_1(k)$ and $C_2(k)$ in front of the integrals are expressed in terms of the dimensionless quantity K_{av}^2. For zinc blende and wurtzite structures we have respectively

$$K_{av}^2 = \frac{e_{14}^2}{\epsilon_0\epsilon_r}\left(\frac{12}{35c_L} + \frac{16}{35c_T}\right) \qquad K_{av}^2 = \frac{e_L^2}{c_L\epsilon_0\epsilon_r} + \frac{e_T^2}{c_T\epsilon_0\epsilon_r}.$$

The longitudinal and transverse elastic constants c_{L} and c_{T} can be obtained from the elastic coefficients c_{11}, c_{12}, and c_{44} or from the longitudinal and transverse sound velocities v_{sL} and v_{sT}, if known.

$$c_{\mathrm{L}} = 0.6\cdot c_{11} + 0.4\cdot c_{12} + 0.8\cdot c_{44}; \qquad v_{\mathrm{sL}} = \sqrt{c_{\mathrm{L}}/\rho}$$
$$c_{\mathrm{T}} = 0.2\cdot c_{11} - 0.2\cdot c_{12} + 0.6\cdot c_{44}; \qquad v_{\mathrm{sT}} = \sqrt{c_{\mathrm{T}}/\rho}$$

The piezo coefficients e_{15}, e_{31}, and e_{33} are used to calculate the corresponding e_{L}^2 and e_{T}^2, which are necessary to obtain the coupling coefficient K_{av} taking into account the wurtzite structure.

$$e_L^2 = \frac{e_{33}^2}{7} + \frac{4e_{33}(e_{31}+2e_{15})}{35} + \frac{8(e_{31}+2e_{15})^2}{105};$$
$$e_T^2 = \frac{16e_{15}^2}{35} + \frac{16e_{15}(e_{33}-e_{31}-e_{15})}{105} + \frac{2(e_{33}-e_{31}-e_{15})^2}{35}.$$

Selection of the after-scattering state. Since $\cos\theta$ is uniquely determined by the value of q, the main task is to derive algorithm for selection of q. The angle ϕ is then selected randomly. ϕ, $\cos\theta$ and q determine $\mathbf{q}$, and the after-scattering state is given by $\mathbf{k}' = \mathbf{k} + \mathbf{q}$. The probabilities P_1 and $P_2 = 1 - P_1$ for the after scattering state to be selected by the corresponding terms which comprise λ_e are

$$\lambda_a = C_1 I_1 + C_2 I_2; \qquad P_1 = \frac{C_1 I_1}{C_1 I_1 + C_2 I_2}; \qquad P_2 = \frac{C_2 I_2}{C_1 I_1 + C_2 I_2}$$

Furthermore, to select q by either term we have to solve the equality $I_i(x_r, x_1) = rI_i(x_2, x_1)$; where r is a random number and q is determined from $q = x_r q_0$. Neither of these equations can be solved for x_r in a simple way. The problem can be overcome by application of a rejection technique: The value of x_r is generated by using a function $\xi_i(x)$ greater than the corresponding integrand J_i. Then, depending on the non equality $\xi_i(x_r)r' < J_i(x_r)$, where r' is a second random number, the value of x_r is accepted or rejected.

For the first case we choose $\xi_1(x) = \frac{x}{x^2+2}$, $\xi_1(x) > J_1(x) \forall x$ (Fig. 1). This choice gives the following expression for x_r:

$$x_r^2 = (x_2^2 + 2)^r (x_1^2 + 2)^{1-r} - 2$$

In the second case we choose $\xi_2(x) = \frac{x}{\sqrt{x^2+4}}$, $\xi_2(x) > J_2(x) \forall x$ (Fig. 2) so that:

$$x_r^2 = \left(r\sqrt{x_2^2 + 4} + (1 - r)\sqrt{x_1^2 + 4} \right)^2 - 4$$

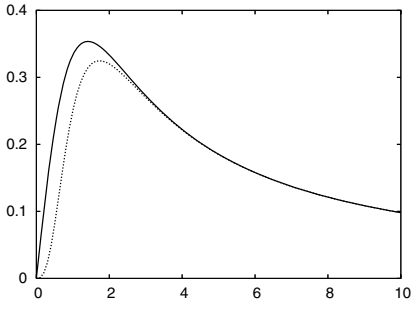

Fig. 1. The function ξ_1 (solid line) as compared to J_1 (dots)

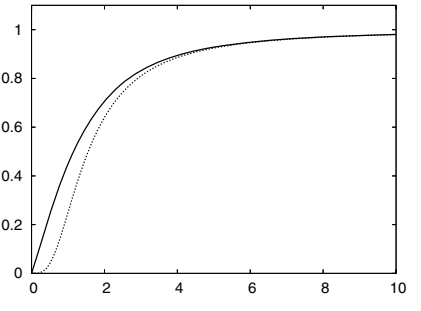

Fig. 2. The function ξ_2 (solid line) as compared to J_2 (dots)

2.2 Emission

The necessary condition for emission is the initial electron energy to be greater than the phonon energy: $\epsilon(k) > \hbar\omega_q$. The out-scattering rate is calculated in the same way as in the case of absorption. In particular the delta function gives rise to the relation:

$$\cos\theta = \frac{2v_s}{v(k)} + \frac{q}{2k}(1 - 4\alpha\epsilon_s); \tag{2}$$

giving rise to the condition $q_1 \leq q \leq q_3$, where
(i) if $\frac{v_s}{v} < 1$ then $\frac{v_s}{v} \leq \cos\theta \leq 1$ and $q_1 = 0$, $q_3 = \frac{2k(1-v_s/v)}{1-4\alpha\epsilon_s}$;
(ii) else there is no solution.
Thus, the out-scattering rate is evaluated as:

$$\lambda_e = C_1(k)I_1(0, x_3) - C_2(k)I_2(0, x_3)$$

Selection of the after-scattering state. We utilize the condition $C_1 I_1(0, x_3) > \lambda_e$ to develop a rejection technique. Since ξ_1 is a majorant function for J_1, the value of x_r is obtained according to:

$$x_r^2 = (x_3^2 + 2)^r 2^{1-r} - 2$$

A second random number r' is used to accept or reject x_r in the inequality:

$$C_1(k)\xi_1(x_r)r' < C_1(k)J_1(x_r) - C_2(k)J_2(x_r)$$

The functions ξ_1 and ξ_2 are compared on Figs. 1 and 2 with the corresponding counterparts J_1 and J_2. In both cases the difference is negligible for $x = q/q_0 > 3$. At room temperatures the average electron wave vector q is of order of 10^7 [1/cm], while q_0 is usually an order of magnitude smaller. Hence the region of significant rejection, below $x = 3$, is relatively rarely visited during the simulations.

3 Simulation Results

In order to establish a rigorous MC simulation, parameters from various publications have been collected and analyzed [5]. Table 1 provides a summary of bulk material parameters for GaN, necessary for analytical band-structure MC simulations, such as energies of lowest conduction bands, effective electron masses, non-parabolicity factors, and model parameters for the acoustic deformation potential (ADP) scattering, inter-valley scattering (iv), and polar optical phonon scattering (LO). ε_∞ and ε_s are the optical and static dielectric constants, ρ is the mass density.

Table 2 summarizes the values for GaN of the elastic constants c_{11}, c_{12}, and c_{44} together with the piezo coefficients e_{15}, e_{31}, and e_{33} adopted in our MC simulation. From them, the corresponding c_L, c_T, v_sl, v_st, e_L^2, e_T^2, and K_{av} are obtained.

Using the established setup of models and model parameters, we obtained MC simulation results for different physical conditions (doping, temperature, field, etc.) for bulk GaN. Fig. 3 shows the low-field electron mobility in hexagonal

Table 1. Summary of material parameters of wurtzite GaN for Monte Carlo simulation

Bandgap energy			Electron mass			Non-parabolicity			Scattering models					
Γ_1	U	Γ_3	$m_{\Gamma 1}$	m_U	$m_{\Gamma 3}$	$\alpha_{\Gamma 1}$	α_U	$\alpha_{\Gamma 3}$	ADP	$\mathrm{hf}_{\mathrm{iv}}$	$\mathrm{hf}_{\mathrm{LO}}$	ρ	ε_s	ε_∞
[eV]	[eV]	[eV]	[m_0]	[m_0]	[m_0]	[1/eV]	[1/eV]	[1/eV]	[eV]	[meV]	[meV]	[g/cm^3]	[-]	[-]
3.39	5.29	5.59	0.21	0.25	0.40	0.189	0.065	0.029	8.3	91.0	92.0	6.07	8.9	5.35

Table 2. Summary of elastic constants of GaN and the resulting longitudinal and transverse elastic constants and sound velocities

c_{11} [GPa]	c_{12} [GPa]	c_{44} [GPa]	c_{L} [GPa]	c_{T} [GPa]	v_{sl} [m/s]	v_{st} [m/s]	e_{15} [C/m^2]	e_{31} [C/m^2]	e_{33} [C/m^2]	e_{L}^2 [C^2/m^4]	e_{T}^2 [C^2/m^4]	K_{av} [-]
373	141	94	355	103	7641	4110	-0.30	-0.36	1.0	0.106	0.452	0.137

GaN as a function of free carrier concentration. Two MC simulation curves are included to demonstrate the effect of the piezo-scattering model and its impact on the low-field mobility. Our MC simulation is in fairly good agreement with experimental data from collections or single point measurements from [6,7,8,9,10]. The electron mobilities, selected for comparisons in this work, consider bulk material and are measured using the Hall effect. The discrepancy between our simulation results and the measured data might be attributed to dislocation scattering which is not considered in our work. This mechanism is considered to be a source of mobility degradation for GaN samples.

Fig. 4 shows the corresponding scattering rates as a function of the doping concentration in hexagonal GaN. Note, that the piezoelectric scattering is the dominant mobility limitation factor at low concentrations even at room temperature, beside the commonly accepted importance at low temperatures.

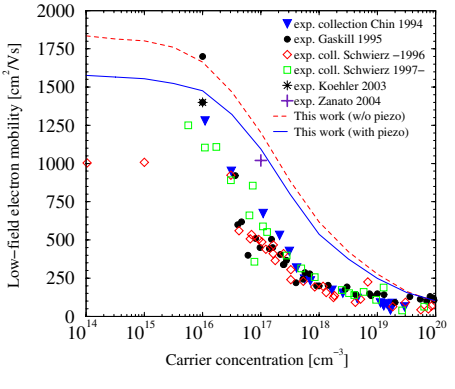

Fig. 3. Low-field electron mobility as a function of carrier concentration in GaN. Comparison of the MC simulation results and experimental data.

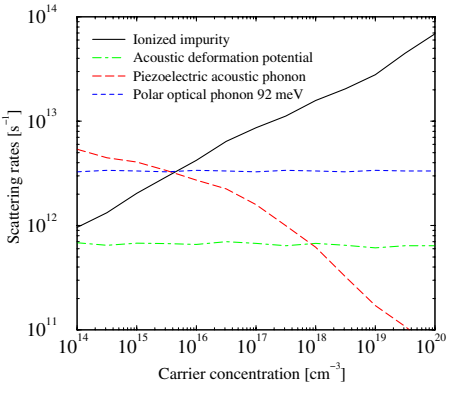

Fig. 4. Scattering rates utilized in our simulation model for wurtzite GaN as a function of carrier concentration at room temperature

Fig. 5 shows the low-field electron mobility as a function of lattice temperature in GaN at 10^{17} cm^{-3} concentration. The experimental data are from [10,11,12]. Note, that mobility increases over the years because of the improved material quality (reduced dislocation density).

Fig. 6 provides the electron drift velocity versus the electric field. We compare our MC results with other simulations [3,13,14,15,16], and with the available experimental data [17,18]. The low field data points are in qualitatively good

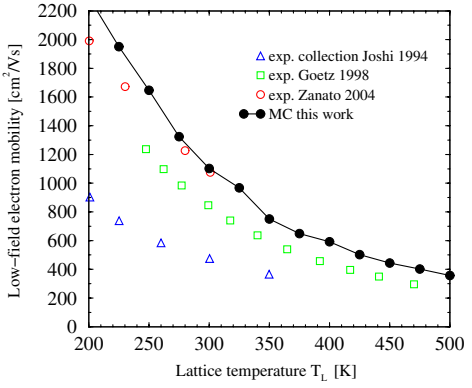

Fig. 5. Low-field electron mobility as a function of lattice temperature in GaN at carrier concentration of 10^{17} cm^{-3}

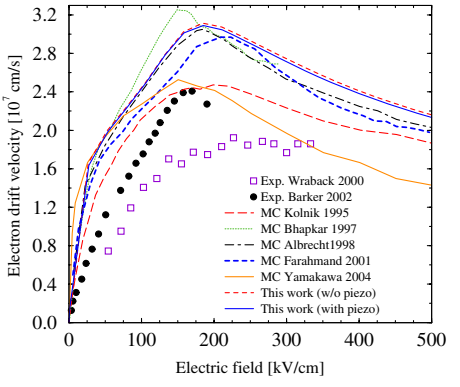

Fig. 6. Drift velocity vs. electric field in wurztite GaN: Comparison of MC simulation results and experimental data

agreement, at higher fields experimental values are significantly lower. Both experiments [17,18] of electron velocities in bulk GaN, employ pulsed voltage sources. The discrepancy in the MC results comes from differently chosen sets of parameter values and considerations of scattering mechanisms.

Our MC results prove that the piezoscattering mechanism has less influence at higher electric fields than other scattering mechanisms, such as polar optical scattering.

4 Conclusion

A non-parabolic piezoelectric model of electron-phonon interaction is derived. It is applied to materials with hexagonal crystal structure in a Monte Carlo simulator. The importance of the piezoelectric effect is illustrated by simulation results for different physical conditions.

Acknowledgment

This work has been supported by the Austrian Science Funds, FWF Project START Y247-N13.

References

1. B. Ridley, Quantum Processes in Semiconductors, Oxford University Press, third ed. (1993).
2. G. Kokolakis, F. Compagnone, A. Di Carlo, and P. Lugli, Exciton Relaxation in Bulk Wurtzite GaN: the role of piezoelectric interaction, Phys. Stat. Sol. (a) **195**, (2003), 618–627.

3. S. Yamakawa, S. Aboud, M. Saraniti, and S. Goodnick, Influence of Electron-Phonon Interaction on Electron Transport in Wurtzite GaN, Semicond. Sci. Technol. **19**, (2004), 475–477
4. O. Madelung, Introduction to Solid-State Theory, Springer Verlag, (1978).
5. V. Palankovski, A. Marchlewski, E. Ungersböck, and S. Selberherr, Identification of Transport Parameters for Gallium Nitride Based Semiconductor Devices, 5th Vienna Symp. on Mathematical Modeling MATHMOD, **2**, AGRESIM-Verlag, Vienna, (2006), 14-1–14-9
6. F. Schwierz, An Electron Mobility Model for Wurtzite GaN, *Solid-State Electron.*, **49**, no. 6, 889–895, 2005.
7. V. Chin, T. Tansley, and T. Osotachn, Electron Mobilities in Gallium, Indium, and Aluminium Nitride, *J.Appl.Phys.*, **75**, no. 11, 7365–7372, 1994.
8. D. Gaskill, L. Rowland, and K. Doverspike, Electrical Properties of AlN, GaN, and AlGaN, in *Properties of Group III Nitrides* (J. Edgar, ed.), no. 11 in EMIS Datareviews Series, section 3.2, 101–116, IEE INSPEC, 1994.
9. K. Köhler, S. Müller, N. Rollbühler, R. Kiefer, R. Quay, and G. Weimann, Multiwafer Epitaxy of AlGaN/GaN Heterostructures for Power Applications, in *Proc. Intl. Symp. Compound Semiconductors*, Lausanne, 235–238, 2003.
10. D. Zanato, N. Balkan, G. Hill, and W. J. Schaff, Energy and Momentum Relaxation of Electrons in Bulk and 2D GaN, *Superlattices & Microstructures*, **36**, no. 4-6, 455–463, 2004.
11. R. Joshi, Temperature-dependent Electron Mobility in GaN: Effects of Space Charge and Interface Roughness Scattering, *Appl.Phys.Lett.*, **64**, no. 2, 223–225, 2004.
12. W. Götz, N. Johnson, C. Chen, H. Liu, C. Kuo, and W. Ilmler, Activation Energies of Si Donors in GaN, *Appl. Phys. Let.*, **6**, no. 22, 3144–3147, 1996.
13. J. Kolnik, I. Oguzman, K. Brennan, R. Wang, P. Ruden, and Y. Wang, Electronic Transport Studies of Bulk Zincblende Wurtzite Phases of GaN Based on an Ensemble Monte Carlo Calculation Including a Full Zone Band Structure, *J.Appl.Phys.*, **78**, no. 2, 1033–1038, 1995.
14. U. Bhapkar and M. Shur, Monte Carlo Calculation of Velocity-Field Characteristics of Wurtzite GaN, *J.Appl.Phys.*, **82**, no. 4, 1649–1655, 1997.
15. J. Albrecht, R. Wang, and P. Ruden, Electron Transport Characteristics of GaN for High Temperature Device Modeling, *J.Appl.Phys.*, **83**, no. 9, 4777–4781, 1998.
16. M. Farahmand, C. Garetto, E. Bellotti, K. Brennan, M. Goano, E. Ghillino, G. Ghione, J. Albrecht, and P. Ruden, Monte Carlo Simulation of Electron Transport in the III-Nitride Wurtzite Phase Materials System: Binaries and Ternaries, *IEEE Trans.Electron Devices*, **48**, no. 3, 535–542, 2001.
17. M. Wraback, H. Shen, J. Carrano, T. Li, J. Campbell, M.J.Schurman, and I. Ferguson, Time-Resolved Electroabsorption Measurement of the Electron Velocity-Field Characteristic in GaN, *Appl. Phys. Let.*, **76**, no. 9, 1154–1157, 2000.
18. J. Barker, R. Akis, D. Ferry, S. Goodnick, T. Thornton, D. Kolesk, A. Wickenden, and R. Henry, High-Field Transport Studies of GaN, *Physica B*, **314**, no. 1-4, 39–41, 2002.